Geometrically nonlinear analysis of planar frame structures with positional finite element method

Antônio Vaz Eduardo Júnior[1], Arthur Álax de Araújo Albuquerque[1], Daniel de Lima Araújo[1]

[1]_School of Civil and Environmental Engineering, Federal University of Goiás_
Av. Universitária N. 1488 - St. Universitário - Goiânia, 74605-220, Goiás, Brazil
antoniovaz@discente.ufg.br, arthuralax@ufg.br, dlaraujo@ufg.br

Abstract. Problems in structural engineering involving geometric nonlinearity are extensively studied from numerical and experimental perspectives. From a numerical modeling perspective, to investigate the resistance mechanisms that arise in structures when subjected to significant displacements, a mathematical formulation that is capable of numerically representing the phenomena that arise during the nonlinear behavior is necessary. This work addresses the problem of planar frame structures involving geometric nonlinearity using a formulation available in the literature of the Finite Element Method (FEM) based on positions and unconstrained vectors as degrees of freedom. In this formulation, nodal positions are used as degrees of freedom of the problem and the Saint-Venant-Kirchhoff constitutive law for the plane stress state is used. Instead of the FEM formulation for displacements, the positional formulation adopted requires strategies for connecting non-collinear finite elements, which involve penalization techniques to satisfy boundary conditions. As described in the literature, connections between non-collinear elements are performed using uniaxial and flexural springs. The strain energies of the springs are determined by the nodal positions of the structure, and their contributions to the Hessian matrix and internal force vector of the structure are calculated using a penalization approach. To validate the implementation developed, solutions of the positional FEM are compared to analytical and numerical solutions obtained by the finite element software DIANA FEA$^{©}$. Furthermore, parametric analyses are carried out to determine minimum stiffness values for the connection springs to allow the representation of the nonlinear equilibrium trajectory of planar frame structures.

Keywords: planar frame structures, positional FEM, geometric nonlinearity.

1   Introduction

The most used FEM formulation, in the field of structural engineering, uses the nodal displacements of the elements as degrees of freedom. Therefore, all quantities involved in the analysis of the structure are derived according to the solution of the system of equations (linear or non-linear, depending on the type of analysis involved) as a function of the calculated nodal displacements [1]. On the other hand, the positional formulation of the FEM uses the nodal positions of the elements as degrees of freedom and arises from the researchers belonging to the Computational Mechanics Group (GMEC) of the Department of Structural Engineering at the São Carlos School of Engineering [2], such as Coda and Greco [3], Greco *et al*. [4], Coda and Paccola [5], Coda and Paccola [6], Coda and Paccola [7]. Two different kinematics can be adopted to develop the positional frame elements, considering: rotation [8] or unconstrained vectors as degree of freedom Nogueira [2], Soares [9][10], Soares, Paccola and Coda [11], Bernardo [12] and Ribeiro *et al*. [13]. Adopting unconstrained vectors as degree of freedom, the connections between non-collinear elements must be performed by alternative strategies, such as the insertion of uniaxial and flexural springs. This strategy will be used in this work, whose objective is to estimate the stiffness parameters of these springs to represent a rigid connection between the elements.

2 Positional finite element method

2.1 Change of configuration, strain measure and constitutive law

The positional formulation of the FEM is based on the principle of minimum potential energy, in which both the strain energy ($\mathbb{U}$) of the structure and the potential ($\mathbb{P}$) of the external forces (F_i^α, q_i^β and b_i^γ) are given as functions of the nodal positions, as in eq. (1):

$$\delta\Pi = \delta\left(\mathbb{U} + \mathbb{P}\right) = \delta\left[\int_{V_0} u_e\, dV_0 - F_i^\alpha Y_i^\alpha - \int_{S_\beta} q_i^\beta\left(S_\beta\right) y_i^{(\beta)}\left(S_\beta\right) dS_\beta - \int_{\Omega_\gamma} b_i^\gamma\left(\Omega_\gamma\right) y_i^\gamma\left(\Omega_\gamma\right) d\Omega_\gamma\right] = 0. \quad (1)$$

The change of configuration in a two-dimensional solid is given by the composition of the mapping functions of the initial ($\vec{f}^0$) and current ($\vec{f}^1$) configurations of the body in the parametric coordinates ξ_1 and ξ_2, which can be seen in Figure 1.
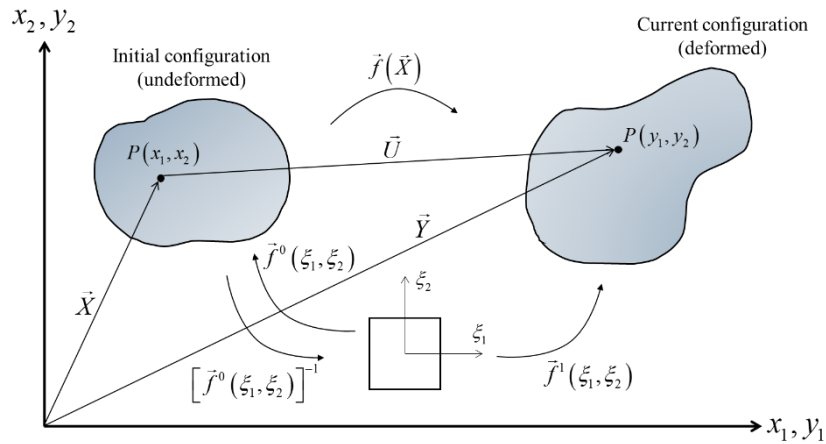
Figure 1 – Change in configuration of a two-dimensional solid

The configuration change function $\vec{f}$ and its respective gradient $\mathbf{A}$ are given by eq. (2) and eq. (3):

$$\vec{f}\left(\xi_1,\xi_2\right) = \vec{f}^1\left(\xi_1,\xi_2\right) \circ \left[\vec{f}^0\left(\xi_1,\xi_2\right)\right]^{-1}, \quad (2)$$

$$\mathbf{A}\left(\xi_1,\xi_2\right) = \nabla\vec{f}\left(\xi_1,\xi_2\right) = \mathbf{A}^1\left(\xi_1,\xi_2\right)\left[\mathbf{A}^0\left(\xi_1,\xi_2\right)\right]^{-1}. \quad (3)$$

The strain measure used in the present work is the Green-Lagrange strain $\mathbf{E}$, which is defined based on the right Cauchy-Green $\mathbf{C}$ strain tensor [15], as presented in eq. (4). The right Cauchy-Green strain tensor can be written in terms of the gradients of the initial and current mapping functions, as detailed in eq. (5):

$$\mathbf{E} = \frac{1}{2}\left(\mathbf{C} - \mathbf{I}\right), \quad (4)$$

$$\mathbf{C} = \left(\mathbf{A}^0\right)^{-T}\left(\mathbf{A}^1\right)^T \mathbf{A}^1\left(\mathbf{A}^0\right)^{-1}. \quad (5)$$

The constitutive law adopted in this work is Saint-Venant-Kirchhoff, given based on the elastic constitutive tensor $\mathfrak{C}$ and the Green strain tensor $\mathbf{E}$, according to eq. (6).

$$u_e = \frac{1}{2}\mathbf{E}:\mathfrak{C}:\mathbf{E}, \quad (6)$$

Associated with the Saint-Venant-Kirchhoff constitutive law and Green's strain, there is the second Piola-Kirchhoff stress tensor $\mathbf{S}$ [15], given by eq. (7):

$$\mathbf{S} = \mathfrak{C} : \mathbf{E} = \frac{\partial u_e}{\partial \mathbf{E}} \tag{7}$$

2.2 Two-dimensional frame element with unconstrained vectors

The positional formulation of a two-dimensional frame element with the use of unconstrained vectors as degrees of freedom, used in this work, can be found in Coda and Paccola [6], Nogueira [2] and Coda [14]. A two-dimensional frame element in its initial and current configurations is illustrated in Figure 2. The mapping functions aim to formulate the frame element based on a reference line associated with a two-dimensional element. The orthogonal vectors $\vec{v}^{\ell}$ at each node ℓ of the frame element, in its initial configuration, are determined from the relative orientation between the reference line and the faces of the two-dimensional element that represent the cross-section associated with the frame element. The unconstrained vectors $\vec{g}^{\ell}$, however, are related to the current configuration of the frame element and do not have the imposition of being orthogonal to the reference line.
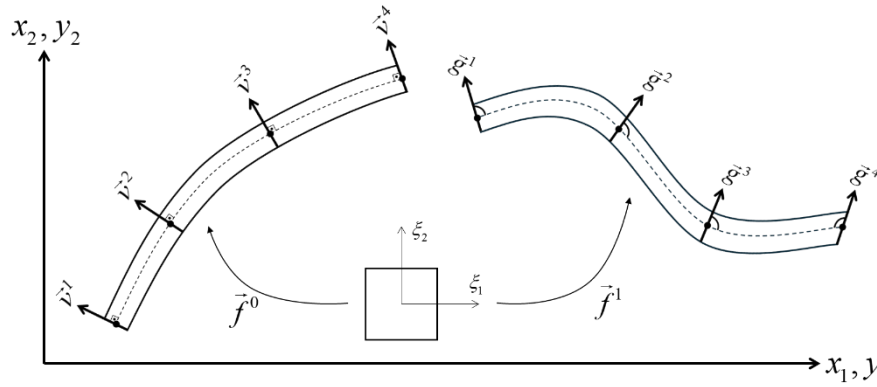
Figure 2 - Mapping of the initial and current configurations of the element

The mapping function of the initial configuration $\vec{f}^{0}$ of the element and its respective gradient $\mathbf{A}^{0}$ [14] are given by eq. (8) and eq. (9):

$$\vec{f}^{0}(\xi_1, \xi_2) = x_i = \varphi_{\ell}(\xi_1) X_i^{\ell m} + \frac{h_0}{2} \xi_2 \varphi_{\ell}(\xi_1) v_i^{\ell}, \tag{8}$$

$$\mathbf{A}^0 = \begin{bmatrix} \dfrac{\partial x_1}{\partial \xi_1} & \dfrac{\partial x_1}{\partial \xi_2} \\ \dfrac{\partial x_2}{\partial \xi_1} & \dfrac{\partial x_2}{\partial \xi_2} \end{bmatrix} = \begin{bmatrix} \left(\varphi_{\ell,1} X_1^{\ell} + \dfrac{h_0}{2} \xi_2 \varphi_{\ell,1} v_1^{\ell} \right) & \left(\dfrac{h_0}{2} \varphi_{\ell} v_1^{\ell} \right) \\ \left(\varphi_{\ell,1} X_2^{\ell} + \dfrac{h_0}{2} \xi_2 \varphi_{\ell,1} v_2^{\ell} \right) & \left(\dfrac{h_0}{2} \varphi_{\ell} v_2^{\ell} \right) \end{bmatrix}, \tag{9}$$

where v_i^{ℓ}, h_0 and φ_{ℓ} are the orthogonal vector at the ℓ-node, the cross-sectional height and the shape function of the frame element, respectively.

Similarly, the mapping function of the current configuration $\vec{f}^{1}$ of the element and its respectively gradient $\mathbf{A}^{1}$ [14] are given by eq. (10) and eq. (11):

$$\vec{f}^{1}(\xi_1, \xi_2) = y_i = \varphi_{\ell}(\xi_1) Y_i^{\ell} + \frac{h_0}{2} \xi_2 \varphi_{\ell}(\xi_1) g_i^{\ell}, \tag{10}$$

$$\mathbf{A}^1 = \begin{bmatrix} \dfrac{\partial y_1}{\partial \xi_1} & \dfrac{\partial y_1}{\partial \xi_2} \\ \dfrac{\partial y_2}{\partial \xi_1} & \dfrac{\partial y_2}{\partial \xi_2} \end{bmatrix} = \begin{bmatrix} \left(\varphi_{\ell,1} Y_1^{\ell} + \dfrac{h_0}{2} \xi_2 \varphi_{\ell,1} g_1^{\ell} \right) & \left(\dfrac{h_0}{2} \varphi_{\ell} g_1^{\ell} \right) \\ \left(\varphi_{\ell,1} Y_2^{\ell} + \dfrac{h_0}{2} \xi_2 \varphi_{\ell,1} g_2^{\ell} \right) & \left(\dfrac{h_0}{2} \varphi_{\ell} g_2^{\ell} \right) \end{bmatrix}, \tag{11}$$

where v_i^{ℓ} is the unconstrained vector at the ℓ-node of the frame element.

2.3 Connection between non-collinear elements

The connection between two elements is shown in Figure 3. For non-collinear elements, Nogueira [2] proposed a spring model that allows representing both perfectly rigid connections, hinged connections or even semi-rigid connections, which is used in this work. The model couples the nodal positions through uniaxial springs and the unconstrained vectors through rotational springs. The strain energy accumulated by uniaxial springs is measured from the relative displacements of the nodes, while rotation springs use the angular variation between the unconstrained vectors. The coupling model adopted is based on the penalization method for imposing the coupling restrictions, which consists of adding additional terms to the system's equilibrium equations (essentially, contributions to the Hessian matrix and internal force vector), which penalize deviation from desired boundary conditions.
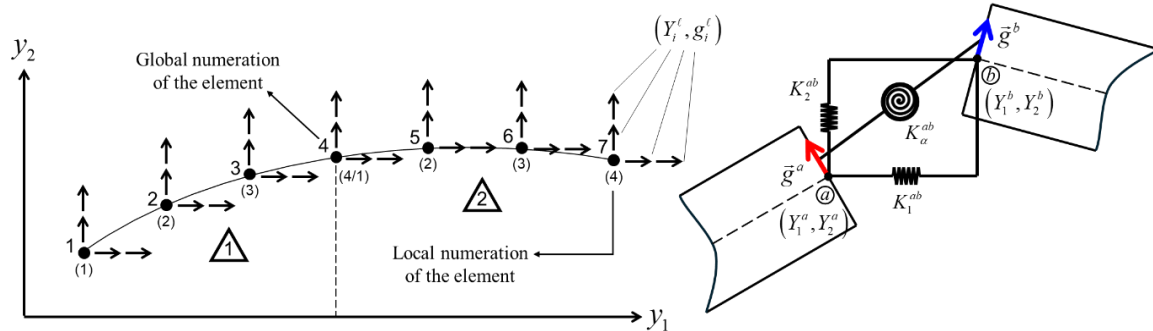
Figure 3 - Connection between non-collinear elements

3 Numerical results and analysis

3.1 Symmetric von Mises's truss

Consider the symmetric von Mises's truss shown in Figure 4. For this structure, two finite elements with linear approximation and unconstrained vectors as degrees of freedom were used. The numerical solution (positional FEM) was obtained using the Newton-Raphson method with displacement control. Furthermore, the structure was modeled and analyzed in the finite element software DIANA FEA$^{©}$ using the CL6TR truss element and considering processing with geometric nonlinearity. A parametric analysis varying the coupling stiffnesses of the nodal positions K_1^{ab} and K_2^{ab} was performed. The stiffnesses ranged from $0.01\mathbb{E}A/\ell_0$ to $100\mathbb{E}A/\ell_0$. Figure 5 shows the deformed shape of the truss and the nonlinear equilibrium trajectories for the different stiffness values adopted. There is a great influence of the stiffness of the uniaxial springs coupling the non-collinear bar elements. It has been observed that for low stiffness values, such as $0.01\mathbb{E}A/\ell_0$, there is virtually no transmission of force between the elements. As the stiffness, or penalty factor, increases, the behavior of the structure converges towards the analytical solution. The response obtained via positional FEM coincides with both analytical and DIANA FEA$^{©}$ solutions when adopting the stiffness around $100\mathbb{E}A/\ell_0$. For stiffness of $\mathbb{E}A/\ell_0$, the difference between the maximum positive and negative force obtained from an analytical solution is up to 36.4%.
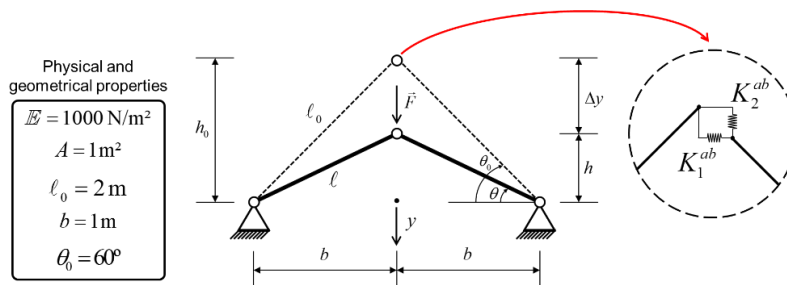
Figure 4 - Symmetric von Mises's truss
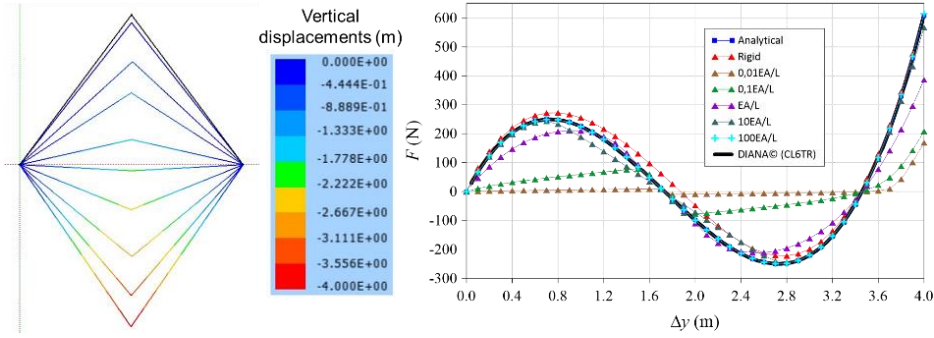
Figure 5 - Vertical displacements and non-linear equilibrium trajectories of symmetrical von Mises's truss

3.2 Asymmetric von Mises's truss

Consider the asymmetric von Mises's truss shown in Figure 6. The same number and type of finite element was used for both the numerical solution via positional FEM and the solution using the DIANA FEA$^{©}$. Both solutions were also based on the Newton-Raphson method with displacement control. The same parametric analysis regarding the stiffness of the coupling springs of the nodal positions was carried out. The deformed shape as well as the nonlinear equilibrium trajectories for both the horizontal u and vertical v displacements of the asymmetric von Mises's truss are presented in Figure 7. As shown in the previous example, the stiffness of the uniaxial springs has a significant influence. The value of the stiffness parameters K_1^{ab} and K_2^{ab} that ensure the rigid connection between the bar elements is also around $100\mathbb{E}A/\ell_0$. However, when compared to the previous example, stiffness values K_1^{ab} and K_2^{ab} close to $10\mathbb{E}A/\ell_0$ already provide adequate results. This behavior can be explained by the asymmetry of the truss, which also develops accentuated displacements in the horizontal direction u. This means that the connection between the elements depends on more of both stiffness parameters, meaning that reduced values of stiffness parameters can be used to obtain an adequate behavior. For the stiffness of $\mathbb{E}A/\ell_0$, the discrepancy between the maximum positive and negative force obtained from an analytical solution amounts to 18.9%.
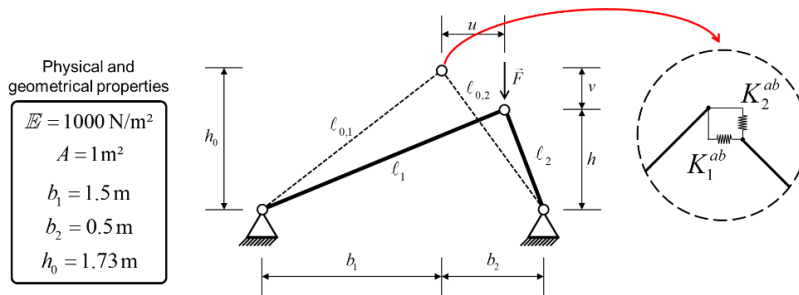
Figure 6 - Asymmetric von Mises's truss
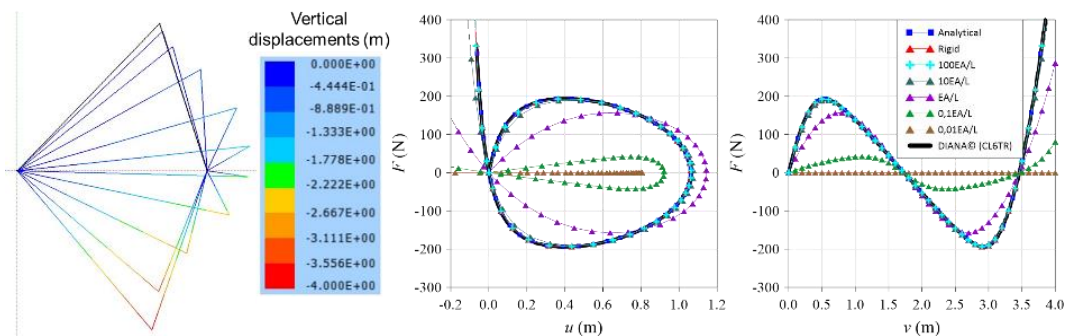
Figure 7 - Vertical displacements and non-linear equilibrium trajectories of asymmetrical von Mises's truss

3.3 Simply supported frame with concentrated force

The frame presented in Figure 8 was modeled in positional FEM using 8 elements with cubic approximation. A concentrated force F is applied to 3/4 of the span of the frame. The bar elements that make up the structure have a rectangular transversal cross-section of dimensions b and h, and are positioned according to their axis of greatest inertia.
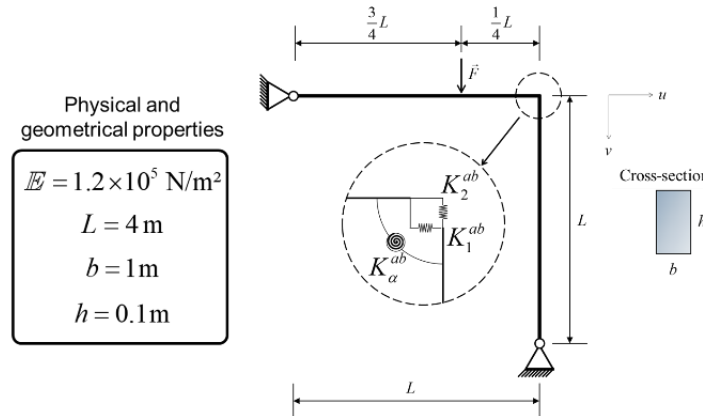
Figure 8 - Simply supported frame with concentrated force

For the uniaxial springs coupling the nodal positions K_1^{ab} and K_2^{ab}, the values of $100\mathbb{E}A/L$ were adopted for their stiffness to consider a rigid displacement connection. For the rotation spring that couples the unconstrained vectors K_α^{ab}, a parametric analysis was carried out to determine the value of the stiffness parameter that represents a rigid connection between the elements. The numerical solution via positional FEM was obtained using the Newton-Raphson method with force control for the solution of the system of nonlinear equilibrium equations. The simply supported frame was also modeled in the DIANA FEA© using eight CL9BE type elements with geometric nonlinearity. The deformed shape of the frame, and its nonlinear equilibrium trajectories for both the horizontal u and vertical v displacements, for each different values of K_α^{ab}, are illustrated in Figure 9. It is observed that the non-linear equilibrium trajectories obtained from positional FEM (Figure 9) present good agreement with the solution using the DIANA FEA© up to force around 6 N. Regarding the unconstrained vectors coupling springs, it is observed that, for low values of rotational stiffness, up to $\mathbb{E}I/L$, the structure tends to present a more reduced resistance and a maximum force up to 28.8% lower than the solution obtained by DIANA FEA©. A similar behavior would be expected if the structure was hinged. When the rotational stiffness increases to $10\mathbb{E}I/L$, the behavior of the structure converges to the solution obtained by DIANA FEA©.
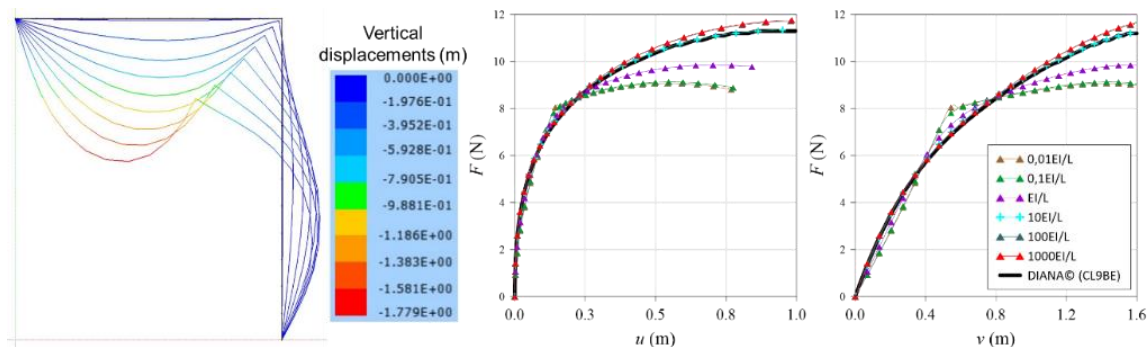
Figure 9 - Vertical displacements and non-linear equilibrium trajectories of simply supported frame

4   Conclusions

The adopted positional MEF formulation, using unconstrained vectors, requires a connection strategy for non-collinear elements. The strategy used in this work consists of connecting these vectors through rotational

springs, in addition to coupling the nodal positions through uniaxial springs. When introducing springs into the connections, the advantage is that, depending on the spring stiffness value, the connection can be represented as a rigid or semi-rigid connection. The definition of the spring stiffness parameter is associated with the degree of stiffness of the connection. Considering very exaggerated stiffness values, in order to consider a rigid connection, can lead to a poor conditioning of the Hessian matrix, which can make it impossible to solve the system of equations (a problem not observed in the examples studied).

The analysis of the results presented in the previous section shows the behavior of the examples studied when faced with a parametric analysis of the stiffness parameters that couple the degrees of freedom (positions and unconstrained vectors) of the non-collinear elements. For the calculated structures, it was possible to determine a stiffness parameter that ensures adequate connection behavior, from small to large displacements. Furthermore, the results showed good agreement with the analytical solutions and the solutions obtained from DIANA FEA$^{©}$.

Authorship statement. The authors hereby confirm that they are the sole liable persons responsible for the authorship of this work, and that all material that has been herein included as part of the present paper is either the property (and authorship) of the authors, or has the permission of the owners to be included here.

References

[1] Rao, S. S. The Finite Element Method in Engineering. Elsevier, 2005.
[2] Nogueira, G. V. Formulação de elemento finito posicional para modelagem numérica de pórticos planos constituídos por compósitos laminados: uma abordagem não linear geométrica baseada na teoria Layerwise. Dissertação (Mestrado em Engenharia de Estruturas), Escola de Engenharia de São Carlos, Universidade de São Paulo, São Carlos, 2015.
[3] Coda, H. B.; Greco, M. A simple FEM formulation for large deflection 2D frame analysis based on position description. Computer Methods in Applied Mechanics and Engineering, v. 193, n. 33–35, p. 3541–3557, ago. 2004.
[4] Greco, M. *et al*. Nonlinear positional formulation for space truss analysis. Finite Elements in Analysis and Design, v. 42, n. 12, p. 1079–1086, ago. 2006.
[5] Coda, H. B.; Paccola, R. R. An Alternative Positional FEM Formulation for Geometrically Non-linear Analysis of Shells: Curved Triangular Isoparametric Elements. Computational Mechanics, v. 40, n. 1, p. 185–200, 28 mar. 2007.
[6] Coda, H. B.; Paccola, R. R. A FEM procedure based on positions and unconstrained vectors applied to non-linear dynamic of 3D frames. Finite Elements in Analysis and Design, v. 47, n. 4, p. 319–333, jan. 2011.
[7] Coda, H. B.; Paccola, R. R. A total-Lagrangian position-based FEM applied to physical and geometrical nonlinear dynamics of plane frames including semi-rigid connections and progressive collapse. Finite Elements in Analysis and Design, v. 91, p. 1–15, nov. 2014.
[8] Reis, M. C. J.; Coda, H. B. Physical and geometrical non-linear analysis of plane frames considering elastoplastic semi-rigid connections by the positional FEM. Latin American Journal of Solids and Structures, v. 11, n. 7, p. 1163–1189, dez. 2014.
[9] Soares, H. B. Formulação e implementação numérica para análise de estabilidade de perfis de parede fina via MEF posicional. 2019. 99p. Dissertação (Mestrado), Escola de Engenharia de São Carlos, Universidade de São Paulo, São Carlos, 2019.
[10] Soares, H. B. Desenvolvimento de ferramenta computacional para análise de colapso estrutural pelo Método dos Elementos Finitos Posicional. 2021. 161p. Tese (Doutorado), Escola de Engenharia de São Carlos, Universidade de São Paulo, São Carlos, 2021.
[11] Soares, H. B.; Paccola, R. R.; Coda, H. B. Unconstrained Vector Positional Shell FEM formulation applied to thin-walled members instability analysis. Thin-Walled Structures, v. 136, p. 246–257, 2019.
[12] Bernardo, C. C. L. G. Enriquecimento da cinemática em elementos finitos de pórticos planos laminados para a regularização das tensões cisalhantes em análise geometricamente não linear. 2021. 109p. Dissertação (Mestrado em Engenharia de Estruturas) – Departamento de Engenharia de Estruturas, Escola de Engenharia de São Carlos, Universidade de São Paulo, São Carlos, 2021.
[13] Ribeiro, L. R. *et al*. Optimal risk-based design of reinforced concrete beams against progressive collapse. Engineering Structures, v. 300, p. 117158, fev. 2024.
[14] Coda, H. B. O método dos elementos finitos posicional: sólidos e estruturas - não linearidade geométrica e dinâmica. EESC-USP, 2018.
[15] Reddy, J. N. An Introduction to Nonlinear Finite Element Analysis. New York: Oxford University Press, 2004.
[16] Crisfield, M. A. Non-linear Finite Element Analysis of Solids and Structures: essentials. New York: John Wiley & Sons, 1991.